Silver nanowire particle reactivity with human monocyte-derived macrophage cells: intracellular availability of silver governs their cytotoxicity

Ioannis G. Theodorou[1,‡], Karin H. Müller[2,‡], Shu Chen[3], Angela E. Goode[1], Vladimir Yufit,[4] Mary P. Ryan[1], Alexandra E. Porter[1]**

[1]Department of Materials and London Centre for Nanotechnology, Imperial College London, Exhibition Road, London SW7 2AZ, United Kingdom

[2]Cambridge Advanced Imaging Centre, Dept. of Physiology, Development and Neuroscience, University of Cambridge, Downing Street, Cambridge CB2 3DY, United Kingdom

[3]Department of Biological Sciences and Institute of Structural and Molecular Biology (ISMB), Birkbeck College, University of London, Malet Street, London, WC1E 7HX, United Kingdom

[4]Department of Earth Science & Engineering, Imperial College London, Exhibition Road, London SW7 2AZ, United Kingdom

KEYWORDS silver nanowires; macrophages; biotransformation; analytical electron microscopy; 3D tomography.

ABSTRACT Silver nanowires (AgNWs) are increasingly being used in the production of optoelectronic devices, with manufacturing processes posing a risk for occupational exposures *via* inhalation. Although some studies have explored the environmental effects of AgNWs, few data exist on human health effects. Alveolar macrophages are central in the clearance of inhaled fibers from the lungs, with frustrated phagocytosis often stated as a key determinant for the onset of inflammatory reactions. However, the mechanisms through which fully ingested AgNWs interact with, degrade and transform within primary macrophages over time, and whether the reactivity of the AgNWs arises due to ionic or particulate effects, or both, is poorly understood. Here, a combination of elemental quantification, 3D tomography, analytical transmission electron microscopy (TEM), and confocal microscopy were employed to monitor the uptake, intracellular Ag^+ availability and processing of AgNWs of two different lengths (1 and 10 μm) inside human monocyte-derived macrophages (HMMs). Using $AgNO_3$ and spherical silver nanoparticles (AgNPs) as a comparison, the amount of total bioavailable/intracellular Ag highly correlated to the cytotoxicity of AgNWs. The 10 μm AgNWs were completely internalized in HMMs, with numerous lysosomal vesicles observed in close vicinity to the AgNWs. Following cellular uptake, AgNWs dissolved and transformed intracellularly, with precipitation of AgCl as well as Ag_2S. These transformation processes were likely due to AgNW degradation in the acidic environment of lysosomes, leading to the release of Ag^+ ions that rapidly react with Cl- and SH- species of the cell microenvironment. Our data suggest that in HMMs, not only frustrated phagocytosis, but also the extent of intracellular uptake and dissolution of AgNWs dictates their cytotoxicity.

Introduction

Silver nanowires (AgNWs) have attracted increasing attention due to their unique physicochemical properties, and are considered as potential building blocks for the next generation of optoelectronic and sensing devices.[1] The increasing use of AgNWs has been accompanied by growing concerns about their potential adverse effects on human health upon exposure. During manufacturing, silver nanomaterials (AgNMs) can be present in liquid and powder forms and potentially present a health risk to workers; in an industrial manufacturing facility, significant release of AgNMs was observed from the reactor, dryer and grinder during a liquid-phase production process, particularly when opening the reactor hatch.[2] The number of particles released from the liquid phase was larger than that emitted during the handling of dried particles, leading to possible occupational exposure even for wet production processes.[2] Although some studies have examined the effects of AgNWs in marine organisms,[3, 4] or animal cell lines,[5] few data exist on their human health effects.[6] Therefore, AgNWs as potential occupational hazards need to be further assessed.

One of the primary routes for exposure is inhalation of airborne AgNWs. Upon inhalation, the nanometer scale of the AgNW diameter defines their aerodynamic properties and allows for preferential deposition in the deep alveolar region of the lung.[7] Several studies have already shown that AgNWs are able to access the alveoli in the deep lung *in vivo*.[5, 8, 9] In the deep lung, alveolar macrophages are central in the clearance of particles by phagocytosis, and the coordination of immune and inflammatory responses. Consequently, macrophages have been widely studied to address their role in fiber-related lung disease,[5, 8, 10-12] but the mechanisms by which AgNWs interact with primary macrophage cells and how AgNWs dissolve and transform within these cells over time is poorly understood.

In the literature, frustrated phagocytosis (occurring when macrophages attempting to phagocytose very long fibers are unable to fully enclose them) has been stated as a key determinant for the onset of inflammatory reactions.[5] Backscattered electron microscopy showed that, following intra-pleural instillation, AgNWs with a length >10 μm may have led to frustrated phagocytosis, while most of the shorter AgNWs (<5 μm) were fully internalized by pleural macrophage cells.[5] Interestingly, AgNWs with lengths of both 5 and 10 μm led to an aggregation of inflammatory cells on the surface of the parietal pleura with accumulation of AgNWs within the lesion area, whereas these effects were not seen only for very short (3 μm) AgNWs.[5] This observation indicates that frustrated phagocytosis is not *solely* responsible for the onset of an inflammatory reaction after exposure to fibrous particles and that, although shorter fibers can be fully phagocytosed, they could still cause sufficient cellular stress to induce pro-inflammatory effects. Although AgNWs were imaged within membrane bound vesicles and in the pleural space, the technique used did not allow for any quantitative analysis of dissolution or changes to the AgNW chemistry or structure after cellular uptake.[5] In addition, no technique capable of unambiguously confirming that the AgNWs were fully internalized by the cells (*e.g.* 3-dimensional (3D) tomography) was used. Another study has also shown that length-dependent frustrated phagocytosis by macrophages following intratracheal instillation of rats with AgNWs (2 and 20 μm) correlated with inflammation.[8] Quantification of Ag-positive macrophages confirmed that silver was present in the macrophages through to day 21 post-exposure, however the exact chemical state of silver contained within the macrophages was not determined.[8] In contrast to these findings, we have recently shown that, following instillation of 1.5 μm and 10 μm AgNWs in Sprague−Dawley rats, individual, intact alveolar macrophages contained AgNWs at 24 h and 7 days after instillation, suggesting that no frustrated phagocytosis had occurred.[9]

However, uptake and transformation of AgNWs within human alveolar macrophages, and how these correlate to their possible cytotoxicity, still remain to be established.

Indeed, a number of studies already suggest that AgNMs chemically transform during their interaction with/in cells. In human alveolar epithelial cells *in vitro*, our group has shown, using analytical transmission electron microscopy, that Ag^+ ions released from AgNWs tend to complex with sulfur species to form highly insoluble Ag_2S ($K_{sp} = 5.92\times10^{-51}$), significantly limiting the short-term toxicological effects of AgNWs.[13] A study employing synchrotron-based transmission X-Ray microscopy (TXM) and X-ray adsorption near edge spectroscopy (XANES), showed that, during uptake and exocytosis from THP-1 macrophages, 20 nm silver nanoparticles (AgNPs) were gradually transformed, first into Ag-O- and then Ag-S- forms.[14] These transformation processes correlated with key events of cellular toxicity, suggesting that the particulate form of AgNPs and their degraded forms play synergetic roles in mediating AgNP cytotoxicity.[14] Using XANES, Ag^+ ions released from 60 nm AgNPs inside primary *murine* macrophages were shown to form complexes with thiolate groups, with glutathione identified as the most likely ligand.[15]

The aim of the present work is to expand on current *in vitro* and *in vivo* findings to provide spatially resolved maps of potential AgNW transformations inside human monocyte-derived macrophages (HMMs) and, if transformations do occur, how their physicochemical properties evolve as a function of time, using 1 and 10 μm long AgNWs. The use of HMMs in our work allows a better representation of macrophages *in vivo* compared to THP-1 macrophages used in previous studies, which are an immortalized cell line. We hypothesize that, not only frustrated phagocytosis, but also the extent of intracellular uptake and dissolution of AgNWs dictates their cytotoxicity. Our results are compared with exposure to aqueous solutions of $AgNO_3$,

representing free Ag^+ ions, and also spherical AgNPs, which would be expected to have a faster dissolution rate than AgNWs. The purpose of testing the AgNPs was solely to confirm whether the toxicity of AgNMs could be attributed to bioavailable Ag inside the cells, and not to compare shape-dependent cytotoxicity. Cellular uptake and transformation of AgNWs were studied in relation to cell viability, during and following uptake by HMM cells. Inductively coupled plasma optical emission spectroscopy (ICP-OES) was used to quantify the amount of uptake of AgNMs and $AgNO_3$ by cells, and the amount of uptake was correlated to toxicity. A combination of 3D tomography, analytical transmission electron microscopy (TEM) and confocal microscopy were used to monitor the uptake and processing of AgNWs inside HMMs over time and at the point of exposure to cells. Unlike other *in vitro* papers addressing the toxicity of AgNWs, the AgNWs tested here were produced and carefully characterized in-house, to ensure full control over the physicochemical properties of the AgNMs being tested.

Experimental

AgNM synthesis

Silver nanowires (AgNWs) of two different lengths ("short" AgNWs: S-AgNWs and "long" AgNWs: L-AgNWs) were prepared via a modified polyol pathway through the reduction of $AgNO_3$ with ethylene glycol (EG, Sigma-Aldrich, UK) in the presence of poly (vinyl pyrrolidone), (PVP, $M_w \approx 360$ k, Sigma-Aldrich, UK) as described by Theodorou et al.[16] The length of the AgNWs was modified by controlling the molar ratio of PVP to $AgNO_3$. AgNWs were washed by repeated cycles of centrifugation at 10000 g with acetone, ethanol and 3 times with de-ionized (DI) water (Millipore Milli-Q gradient system, >18.2 MΩ), dispersed in DI water in a sealed glass vial and stored at 4°C in the dark. The physicochemical properties of the

PVP-coated AgNWs used in this study have been previously thoroughly characterized in our group.[16]

Silver nanoparticles (AgNPs) with an average size of 50 nm ($AgNP_{50}$) were synthesized via chemical bath reduction, in which trisodium citrate ($Na_3C_6H_5O_7$, Fisher Scientific, UK) served a dual role as both reductant and stabilizer. Briefly, a $AgNO_3$ (1.0×10^{-3} M, Sigma-Aldrich, UK) solution was added into preheated DI water. When the solution reached boiling point, a $Na_3C_6H_5O_7$ (1.0×10^{-3} M) solution was added drop-wise. The color of the solution slowly turned into greyish yellow, indicating the reduction of Ag^+ ions. The solution was heated continuously for an additional 20 minutes, and then cooled to room temperature. In order to remove impurities and excess citrate, the synthesis product was washed by repeated cycles of centrifugation at 10000 g with DI water. The citrate-coated $AgNP_{50}$ were dispersed in DI water in a sealed glass vial and stored at 4^oC in the dark.

The purity of the as-synthesized AgNMs was confirmed by Transmission Electron Microscopy (TEM) Energy Dispersive X-ray Spectroscopy (EDX), to ensure that residual reactants were removed by the washing process and that sulfidation of AgNWs had not occurred in the ambient atmosphere.[17] The concentrations of the AgNM stock solutions on a Ag atom basis were determined by Inductively Coupled Plasma–Optical Emission Spectroscopy (ICP-OES, Thermo Scientific, UK), following digestion of AgNM aliquots in concentrated nitric acid (HNO_3, 69%, Sigma-Aldrich, UK), as follows: S-AgNWs: 6.24 mg/mL; L-AgNWs: 2.13 mg/mL and $AgNP_{50}$: 2.58 mg/mL. Stock solutions of $AgNO_3$ at a concentration of 4 mg/mL were prepared in DI water and used immediately.

Bright Field TEM (BF-TEM) of as-synthesized AgNMs

The morphology of AgNMs was examined by BF-TEM. Aliquots of AgNM stock solutions diluted in DI water were drop-cast on 400 mesh copper (Cu) holey carbon film TEM grids (TAAB, UK) and imaged immediately in a JEOL JEM-2100F, combined with selected area electron diffraction (SAED) and Energy Dispersive X-ray Spectroscopy (EDX, Oxford Instruments). The size distributions of AgNMs were characterized using multiple TEM images and ImageJ software (http://rsb.info.nih.gov/ij/).

Cell culture media

The cell culture media used during this study were: (a) MΦ-SFM (macrophage serum-free medium; Invitrogen #12065074 basal medium, supplemented with 100 U/ml penicillin and 100 μg/ml streptomycin). This medium does not contain any serum supplements; however, it contains some protein in the form of albumin and growth factors. The exact medium formulation is proprietary information. MΦ-SFM is optimized for the culture of HMMs and was used for the culture of cells prior to experiments (see below) and for experiments where cells had to be cultured for longer periods of time. (b) RPMI (RPMI-1640 basal medium, Gibco # 11835-030, supplemented with 100 U/ml penicillin and 100 μg/ml streptomycin). This medium did not contain any protein additions and was generally used for shorter incubation periods. The formulation of RPMI cell culture medium is shown in Supporting Information, Table S1. The cell culture media used for each of the following experiments are summarized in Supporting Information, Table S2.

Isolation and culture of HMMs

Human monocyte-derived macrophages (HMMs) were obtained by in vitro culture of human monocytes isolated from human buffy coat residues (National Blood Service, Cambridge, UK), as described previously.[18] Briefly, monocytes were enriched by centrifugations on Ficoll and Percoll density gradients and seeded on tissue culture plates using MΦ-SFM. After incubation for 1 h at 37 ºC, cells were washed twice with phosphate buffered saline (PBS) to remove any remaining non-adherent cells, and monocytes were cultured at 37 ºC in humidified air/5% CO_2 for at least 6-7 days prior to experiments, renewing the MΦ-SFM culture medium twice a week. For cell exposure experiments, AgNWs were diluted from their aqueous stock solutions into MΦ-SFM or RPMI medium to the concentrations stated in the text. Brief (less that 1 min) sonication at 135W was used to ensure that the AgNWs were homogeneously dispersed in solution prior to cell exposure. We found no evidence that this caused changes in the size distribution of the AgNWs.

Viability assays

Viability of HMMs was assessed in 48-well tissue culture plates using the 3-(4, 5-dimethylthiazol-2-yl)-2,5-diphenyl tetrazolium bromide (MTT) assay. Following incubation of cells with AgNMs in MΦ-SFM medium for 24 h, the cell culture supernatants were removed and cells were incubated at 37 ºC for 2 h with 0.5 mg/mL MTT/MΦ-SFM. After removing the dye solution, 500 µL of dimethyl sulfoxide (DMSO) was added to each well. Plates were incubated for 15 min at room temperature to dissolve the dye, centrifuged at 500 g to sediment any floating cells or particles, and 200 µL of supernatant dye extract was transferred to 96 well plates. Absorbance was measured at 570 nm using an ASYS HiTech Expert Plus plate reader

(Biochrom, UK) and cell viability was expressed as a percentage based on a non-treated (NT) control.

Quantification of AgNM/$AgNO_3$ uptake by HMMs

HMMs were incubated with 10 μg/mL AgNMs or $AgNO_3$ in RPMI cell culture medium for 4 h at 37 ºC or at 4 ºC (on ice). Following incubation, cells were washed three times with 0.9% saline to remove extracellular and unbound AgNMs/$AgNO_3$ and the cells were then lysed in DI-water. Lysates were stored at -20 ºC until further analysis. Aliquots of the cell lysates (100 μL) were digested with 5 mL of a 1:3 mixture of concentrated nitric (HNO_3, 69%,) and hydrochloric (HCl, 37%, Sigma-Aldrich, UK) acids overnight, to digest AgNMs. The samples were diluted 10 times in DI water, yielding clear digest solutions. Their Ag content was determined by ICP-OES with a silver detection limit of 0.6 μg/L. Cellular protein concentrations were analyzed in separate wells using a standard Lowry assay and ICP-OES results were expressed as ppm Ag/mg protein.

Abiotic dissolution study

$AgNO_3$ was incubated in MΦ-SFM cell culture medium at a Ag concentration of 40 μg/mL, for 30 min in the dark, which led to the formation of a white precipitate. To determine the fraction of $AgNO_3$ remaining in solution as ionic Ag^+, aliquots of this mixture were filtered at 13000 g for 30 minutes through 2 kDa centrifuge membranes (Sartorius Stedim VIVACON 500). The amount of Ag^+ in the filtrates was measured by ICP-OES. Next, the formed $AgNO_3$/MΦ-SFM precipitate was collected by centrifugation, washed by repeated cycles of centrifugation

with DI-water, and re-suspended in DI water, to form a stock solution for the abiotic dissolution experiment.

S-AgNWs, L-AgNWs, $AgNP_{50}$ and the $AgNO_3$/MΦ-SFM precipitate were incubated at a concentration of 25 μg/mL from the original stock solutions, in a temperature-controlled dri-block incubator at 37 ^oC for 4 h or 24 h in the dark. The incubation medium was Sodium Perchlorate ($NaClO_4•H_20$; Sigma-Aldrich, >99%; 0.1 M), and its pH was adjusted to 7 or 5, using either Perchloric Acid ($HClO_4$, Sigma-Aldrich, 70%, 99.999% trace metals basis) or Sodium Hydroxide (NaOH, Sigma-Aldrich, anhydrous, 99.99%). Following incubation, aliquots of the samples were centrifuged at 13000 g for 30 minutes through 2 kDa centrifuge membranes to remove solid material. The amount of Ag^+ in the filtrates was measured by ICP-OES. Each experiment was repeated three times and the results are given as the mean and standard deviation of the three repeats.

Preparation of ultrathin sections for STEM analysis of cellular uptake of S-AgNWs by HMMs

HMMs were incubated with 25 μg/mL of S-AgNWs in RPMI for 2 h (= pulse period, during which cells are being exposed to particles). The use of RPMI ensured that the AgNWs did not transform to Ag_2S in the cell culture medium before any interactions with HMM cells.[19] Then, cells were either fixed immediately (= chase period of 0 h) or washed (to remove any non-ingested particles) and further cultured (chased) in MΦ-SFM for 24 h or 7 d (= chase periods of 24 h and 7 d). At these time points, cells were washed twice with 0.9% saline to remove excess particles. Then, samples were fixed with 2% glutaraldehyde/2% formaldehyde in 0.05 M sodium cacodylate buffer (pH 7.2) for 4 h at 4 °C. Fixed cells were scraped, transferred to 1.5 mL Eppendorf tubes and washed 3 x in 0.9% saline and 2x in DI-water. The cell pellets were

dehydrated in graded solutions of ethanol (50%, 70%, 95%, and 100%), for 5 minutes three times in each, and then washed three times, for 10 minutes each, in dry acetronitrile (Sigma). After dehydration, samples were progressively infiltrated with a Quetol-based resin, produced by combining 8.75 g quetol, 13.75 g nonenyl succinic anhydride, 2.5 g methyl acid anhydride, and 0.62 g benzyl dimethylamine (all from Agar Scientific). Samples were infiltrated in a 50% resin:acetonitrile solution for 2 h, in a 75% resin:acetonitrile solution overnight and in 100% resin for 4 days, with fresh resin being replaced daily. The embedded samples were cured at 60 ^{o}C for 24 h. Ultrathin sections (70 nm) were cut from the resin blocks directly into a water bath using an ultramicrotome and a diamond knife with a wedge angle of 35 ^{o}. Sections were immediately collected on bare, 300 mesh copper TEM grids (Agar Scientific), dried and stored under vacuum until analysis.

Preparation of whole cells for STEM analysis of cellular uptake of L-AgNWs by HMMs

HMMs were seeded on formvar-coated gold TEM grids and cultured in RPMI for 24 h to allow spreading of the cells on the formvar film. Cells were then exposed to 25 μg/mL of L-AgNWs in RPMI for a 2 h pulse treatment to allow particle uptake, and subsequently washed to remove any non-ingested AgNWs. Then, HMMs were cultured for a further one hour in RPMI to allow surface-bound or partly ingested particles to be internalized. After a brief wash, cells were then cultured for up to 7 d in MΦ-SFM medium. Cells were plunge-frozen using a Leica EM CPC cryofixation system and then freeze-dried overnight using a liquid nitrogen-cooled EMITECH K755X turbo pump.

HAADF-STEM and EDX analysis of cell samples

High angle annular dark field scanning transmission electron microscopy (HAADF-STEM) was performed at 80 kV on a FEI Titan 80–300 TEM/STEM, fitted with a Cs (image) corrector and a SiLi Energy Dispersive X-Ray (EDX) spectrometer (EDAX, Leicester UK). A convergence semi-angle of 14 mrad was used, with inner and outer HAADF collection angles of 49 and 239 mrad, respectively. The probe diameter was <0.5 nm. For L-AgNWs in whole cells, HAADF tomography datasets were acquired over a tilt range of -57 ° to +70 °at 1° increments. Datasets were processed using Inspect 3D software (FEI, v3.0) for tilt series alignments and 3D reconstruction using the simultaneous iterative reconstructions technique (SIRT). Visualisation of the reconstructions was performed by manual segmentation using Avizo 9.0.1 (FEI, USA) and cells were segmented by intensity-based thresholding. The identification of separate nanowires was then carried out by manual inspection. The feret diameters of 22 completely described nanowires were determined using QuiQ 3D (IQM Elements, London, UK) through a hypersphere to fit the nanowires and calculate nanowire length (20). For optimized EDX signal collection, STEM-EDX elemental maps of internalized L-AgNWs were acquired in an FEI image-corrected Titan3 G2 equipped with Quad silicon drift detectors (Super-X) at 300 kV. EDX acquisition and spectral processing including Bremsstrahlung continuum removal and quantification was performed using Esprit 1.9 software (Bruker).

Confocal imaging of L-AgNW uptake and co-localization with lysotracker

For confocal imaging, HMMs were seeded and grown on 35 mm culture inserts (µ-dishes, Ibidi, Germany) using MΦ-SFM medium for about 7 d. Cells were incubated in MΦ-SFM medium only (NT) or with 25 µg/mL L-AgNWs for 2 h at 37 ºC in the presence of 500 µg/mL 10 k-dextran-TexasRed (Molecular Probes, Life Technologies, UK), a fixable fluorescent marker

for lysosomes. Subsequently, cells were washed and fixed for 30 min with 4% formaldehyde in 0.1 M PIPES buffer (pH 7.2). Cell nuclei were counterstained with 10 μg/ml of Hoechst for 5 min. Then, samples were rinsed and embedded using ProLong Gold Antifade (Invitrogen, Life Technologies, UK). Samples were viewed using a Leica SP2 confocal microscope. The 405 nm, 488 nm and 561 nm laser lines were used to image the Hoechst dye, AgNWs (in reflectance mode) and dextran-TexasRed dye, respectively. Image frames were acquired sequentially, using a 63 x water-immersion lens.

Statistics

Toxicity data were analyzed using Analyse-it™ software embedded in Excel. Variations between groups were established using a 1-way Analysis of Variance (ANOVA) and a *Least Significant Difference* (LSD) post hoc test was used to identify homogeneous groups. P values ≤ 0.01 were considered as statistically significant. ICP-OES data were analyzed using a Student's T-test; n = 5.

Results

Characterization of as-synthesized AgNMs

The AgNMs used in this study were synthesized in-house to ensure full control over their physicochemical properties,[16] which are summarized in Table 1. Figure 1 shows the morphology of high-aspect ratio S-AgNWs (Figure 1a, b) and L-AgNWs (Figure 1e, f), which had average lengths of 1.5 ± 1.4 μm (Figure 1c) and 10.5 ± 8.5 μm (Figure 1g), respectively. Both types of AgNWs had similar diameter distributions (Figure 1d, h), with averages of 79 ± 21 nm for S-

AgNWs and 73 ± 37 nm for L-AgNWs. The citrate-capped $AgNP_{50}$ had a round/oval shape (Figure 1, i) with an average diameter of 54 ± 20 nm (Figure 1, j). For citrate-capped $AgNP_{50}$, the lattice spacings measured from selected area electron diffraction (SAED) patterns (Supporting Information, Figure S1a) were 0.236 nm, 0.204 nm, and 0.145 nm, corresponding to the (111), (200) and (220) planes of metallic silver (ref. # 01-087-0597). TEM energy dispersive X-Ray (EDX) spectra collected from areas containing several $AgNP_{50}$ (Supporting Information, Figure S1b) showed that as-synthesized $AgNP_{50}$ consisted of pure Ag, confirming the absence of impurities from the synthesis product and that no sulfidation had occurred on as-synthesized material. The chemistry and crystalline structure of as-synthesized PVP-capped AgNWs has been reported in our previous work.[16]

Furthermore, the cell culture medium (RPMI) used in the present work for quantifying AgNM uptake by HMMs and for HAADF-STEM imaging of the cellular uptake and processing of AgNWs by HMMs, does not induce changes to the their chemistry (*e.g.* sulfidation), as confirmed in our previous work,[19] and using HRTEM and HAADF-STEM for $AgNP_{50}$ (Figure S2). The surface charge of S-AgNWs, L-AgNWs and $AgNP_{50}$ in RPMI (pH 7.2) had slightly lower magnitudes compared to DI water, which may lead to a possibility of some degree of agglomeration in RPMI. This reduction in zeta potentials most likely arises due to a screening effect from the high salt content of the cell culture medium, which decreases the electrostatic repulsive force between particles.[20]

Effect of AgNMs on HMM cell viability

To evaluate the effect of AgNWs on macrophage viability, HMMs were incubated with a dose range of 0-40 μg/mL for 24 h. Their viability was assessed using the MTT assay, which

measures the activity of cellular dehydrogenase enzymes (Figure 2a). As HMMs do not proliferate in culture, any observed drop in formazan production is due to reduced cell viability rather than a drop in cell proliferation. Compared to the non-treated (NT) control, S-AgNWs produced a significant decrease in cell viability at 10, 20 and 40 μg/mL. L-AgNWs significantly decreased cell viability at all concentrations tested (1.25, 2.5, 5 10, 20 and 40 μg/mL). To compare these results with another AgNM that is expected to have a higher dissolution rate than AgNWs, we tested the effect of $AgNP_{50}$ on HMM viability. Although the toxicities of S-AgNWs and L-AgNWs were not significantly different from each other, $AgNP_{50}$ were significantly more toxic than both types of AgNWs, with a decrease in cell viability of about 36 % observed at the highest concentration tested (Figure 2a). To further compare these findings with the toxicity of ionic Ag, HMMs were exposed to silver nitrate ($AgNO_3$) at concentrations corresponding to the same Ag elemental concentrations as AgNMs. $AgNO_3$ was highly toxic to HMMs at all concentrations tested (1.25, 2.5, 5 10, 20 and 40 μg/mL) and significantly more toxic than all types of AgNMs. The estimated median lethal concentrations (LC_{50}, representing a 50% reduction of cell viability, in terms of μg Ag) were 0.09, 27.2, 61.9 and 46.9 μg Ag/mL for $AgNO_3$, $AgNP_{50}$, S-AgNWs and L-AgNWs, respectively.

$AgNO_3$ has frequently been used in previous studies as a control, to represent free ionic Ag^+ and compare its effects to metallic Ag. However, upon addition of $AgNO_3$ (from a stock solution in DI water) to MΦ-SFM cell culture medium prior to addition to the cells, the immediate formation of a precipitate was observed. This precipitate was collected by centrifugation and washed with DI water by repeated cycles of centrifugation, which ensured that any media components were removed prior to analysis. Imaging of the precipitate by BFTEM (Supporting Information, Figure S3a, b) showed that it consisted of small irregular particles.

TEM-EDX confirmed the presence of Cl and S in these particles (Supporting Information, Figure S3c), while SAED showed that the particles were crystalline (Supporting Information, Figure S3d). The interplanar spacings measured from SAED patterns were 0.324 ± 0.005, 0.289 ± 0.004, 0.277 ± 0.003, 0.262 ± 0.004, 0.238 ± 0.004, 0.199 ± 0.005 nm, which are consistent with the cubic form of AgCl (ICSD ref. #01-031-1238) and the monoclinic form of Ag_2S (ICSD ref. #00-014-0072). Therefore, the precipitate likely consisted of a mixture of AgCl and Ag_2S nanoparticles. Inductively coupled plasma optical emission spectroscopy (ICP-OES) was used to measure the amount of remaining ionic Ag^+ in the MΦ-SFM medium, following removal of the precipitate through centrifugal filtration, and was found to be below the detection limit (<0.6 μg/L). Consequently, $AgNO_3$ does not represent a true ionic control. Upon addition to tissue culture media, free Ag^+ is almost entirely sequestered by chloride or sulfide components of the basic media formulation to form insoluble precipitates in the media. In the presence of albumin/serum in these media, Ag^+ may also react with protein thiol groups of these supplements to form Ag_2S-protein adducts, prior to addition to the cells.[21]

Quantification of AgNM uptake by ICP-OES

The differences in cell viability observed after exposure of HMMs to different AgNMs in the cytotoxicity experiment may have various causes: different amounts of Ag materials internalized by the cells; different rates of Ag dissolution; production of different toxic species and different pathways of cell death. In order to test whether the differences in cell viability between Ag compounds arise due to differences in the amounts internalized by the cells, uptake in HMMs was quantified by elemental analysis using ICP-OES. HMMs were incubated with 10 μg/mL AgNMs and $AgNO_3$, at both 4 ^oC and 37 ^oC, for 4 h (Figure 2b). This short exposure

period of 4 h was chosen to eliminate potential effects that uptake saturation and/or declining cell viability due to ingested AgNMs could have on the uptake processes of HMMs. At 4 ^{o}C, particles/ligands are still able to bind on the cell surface but active uptake by the cells is inhibited, whereas at 37 ^{o}C, cells can bind as well as actively internalize particles. Therefore, the difference in uptake between 37 and 4 ^{o}C represents the amount of Ag compound actively ingested by the cells (Figure 2c). For the NT-control, the amount of Ag measured was below the ICP-OES detection limit of 0.6 μg/L. At 4 ^{o}C, the amounts of Ag associated with the cells increased in the order: S-AgNWs < L-AgNWs < $AgNP_{50}$ < $AgNO_3$, and they were all statistically different from each other (Students T-test, p-value ≤ 0.05). The amount of Ag measured after exposure of cells to $AgNO_3$ at 4 ^{o}C is very high compared to the rest of the materials. As mentioned previously, the addition of $AgNO_3$ to culture medium led to the immediate formation of a precipitate composed of Ag, Cl and S (Supporting information, Figure S3). Apart from binding to the cell surface, this precipitate also had a tendency to stick non-specifically to the cell culture plastic (particularly at 4 ^{o}C) and was hard to remove completely through washing before preparation of the cell lysates for ICP-OES. This non-specifically bound Ag precipitate may therefore have contributed to the measurement and the high Ag values observed in this particular sample. These limitations also corroborate with the high standard deviation obtained for the $AgNO_3$ samples, at both 4 ^{o}C and 37 ^{o}C (Figure 2b, c). Since this precipitate consisted of a mixture of AgCl and Ag_2S nanoparticles (Supporting Information, Figure S3), with no ionic Ag^+ remaining in solution after the precipitation, it is highly likely that the toxicity to HMMs was caused by the high uptake of the $AgNO_3$/medium precipitate particles, rather by any remaining, free ionic Ag^+ in the medium. At 37 ^{o}C, the amounts of Ag associated with the cells were significantly higher than those at 4 ^{o}C, demonstrating that all Ag compounds

were actively internalized by HMMs. Active uptake was statistically different between materials and increased in the order: S-AgNWs<L-AgNWs < $AgNP_{50}$ <$AgNO_3$. One reason for the higher active uptake observed for L-AgNWs compared to S-AgNWs may be their larger size, which allows them to sediment more rapidly onto the adherent cells, therefore exposing the cells to higher localized concentrations of particles.[22] In addition, L-AgNWs may be ingested by the cells in larger amounts due to different uptake mechanisms being involved. The L-AgNWs - due to their size - may increasingly be ingested by phagocytosis and macropinocytosis, two uptake pathways very active in HMMs, rather than by endocytosis in smaller vesicles. When the amount of intracellular Ag content was plotted against the measured cytotoxicity (LC_{50} values), a positive linear trend was observed (Figure 2d; $R^2 = 0.988$). Therefore, the magnitude of uptake was clearly correlated with the observed cytotoxic effects; the higher the intracellular Ag content, the higher was the decrease in cell viability.

For all cell exposure experiments, AgNMs were diluted from their aqueous stock solutions into serum-free cell culture media (MΦ-SFM or RPMI) to the concentrations stated in the text. Serum-free culture media were selected, as serum proteins are not expected to exist in an *in vivo* inhalation scenario, with which this study is concerned. The alveoli are covered by a thin layer of pulmonary surfactant (PS), which represents a first line of defense of the lungs against inhaled NMs.[23] Serum proteins are only present in the PS in disease, and are known to inhibit surfactant biophysical activity.[24] As a control, we tested the effect of 5 mg/mL of *bovine* serum albumin (BSA) on the uptake of S-AgNWs (Supporting Information, Figure S4). Albumin did not significantly affect the cell-binding or uptake efficiency for AgNWs, therefore all further experiments were performed in serum-free media.

ICP-OES measures total Ag metal content and cannot distinguish between Ag^+ ions, metallic Ag or other Ag compounds in the cell lysates. In order to predict under which conditions Ag^+ ions might be released from AgNMs and at which rates, we performed an abiotic (cell-free) dissolution study. We used ICP-OES to compare the rates of Ag^+ ion release from 25 μg/mL of AgNWs and $AgNP_{50}$, as well as the precipitate formed upon addition of $AgNO_3$ to MΦ-SFM. All materials were incubated in non-interacting perchlorate buffers with pH 7 and pH 5 that mimic extracellular and lysosomal pH, respectively (Figure 2e). At pH 7, Ag^+ release was negligible for both types of AgNWs up to 24 h, indicating that extracellular dissolution of these AgNMs is unlikely to be a factor in mediating their cytotoxicity. At pH 5, dissolution was not significantly different compared to pH 7 after 4 h. However, after 24 h at pH 5, a significantly higher amount of Ag^+ ions had been released from S-AgNWs and L-AgNWs compared to pH 7, suggesting that dissolution in the acidic compartment of lysosomes could be a pathway for mediating the cytotoxicity observed for AgNWs in our study. Similarly, $AgNP_{50}$ showed a low dissolution rate after 4h and 24h at pH 7. However, $AgNP_{50}$ had a significantly higher dissolution rate at pH 5, both after 4h and 24h, compared to AgNWs. The $AgNO_3$/medium precipitate also showed very low dissolution rates after 4 h and 24 h, both at pH 7 and pH 5, in spite of being highly toxic to HMM. This high toxicity would suggest that intracellular dissolution of the precipitate may take place in HMMs (Supporting Information, Figure S5). In fact, the strong linear correlation found between the cytotoxicity of different types of Ag materials and their degree of active uptake by HMMs, implies that Ag^+ must be released intracellularly at a similar rate by all materials. These findings suggest that the amount of bioavailable/intracellular Ag^+ is a better predictor of cytotoxicity of AgNMs than simply measuring Ag^+ release rates under abiotic conditions, a notion supported by the literature.[25]

HAADF-STEM imaging of the cellular uptake of S-AgNWs by HMMs

High resolution transmission electron microscopy was used to confirm whether the AgNWs had been internalized by the HMMs and whether they had degraded and transformed inside these cells. No heavy metal staining process was used, since it has been shown to alter both the morphology and chemistry of AgNMs,[13] and the inherent contrast of the biological sample is therefore low. Samples were imaged using HAADF-STEM, a technique which is highly sensitive to local variations in the atomic number within a sample (Figure 3), which means Ag-containing compounds will show extremely high contrast. HMMs were co-incubated with S-AgNW for a pulse period of 2 h. At the 0-h time point (fixed immediately after the 2 h pulse period), S-AgNWs were found inside HMMs (Figure 3a). Alterations in the morphology of the S-AgNWs were observed compared to the as-synthesized material and small particles surrounded the tips of the S-AgNWs (Figure 3a, b). STEM-EDX, which allows elemental analysis with resolution at the nanometer scale, revealed the presence of Ag(L), S(K) and Cl(K) peaks in the spectra of these small particles (Figure 3c, spectrum 2), whereas the bulk of the AgNWs was still composed of pure Ag (Figure 3c, spectrum 1). After a 24 h chase period, further degradation of the S-AgNWs led to the formation of a core-shell structure (Figure 3d, e), where the shell was sulfur-rich (Figure 3f, spectrum 4) but the core remained pure Ag (Figure 3f, spectrum 3). After a 7 d chase period, no intact S-AgNWs were found intracellularly (Figure 3g, h), but only sulfur-containing irregular silver nanoscale structures (Figure 3i).

Tomographic imaging of the cellular uptake of L-AgNWs by HMMs

Since 2-dimensional imaging of thin sections provides incomplete information on the length and distribution of L-AgNWs inside cells (due to sectioning of the nanowires and projection issues), 3-dimensional analysis was performed using HAADF-STEM tomography of unsectioned freeze-dried cells in order to accurately monitor the uptake of L-AgNWs by HMMs (Figure 4). Following a 24 h chase period with 25 μg/mL of L-AgNWs, HAADF-STEM imaging of freeze-dried HMMs showed L-AgNWs associated with HMMs (Figure 4a, b). 3D reconstructions of HAADF-STEM tomographic datasets revealed the intracellular distribution of these L-AgNWs, with respect to the plasma membrane and the nucleus, showing that L-AgNWs were completely internalized by the HMM (Figure 4c, d). Quantification of the internalized L-AgNWs from one HMM showed a mean length of 1.8 ±1.6 μm, while the longest fully internalized L-AgNW in this cell measured 7.3 μm. Furthermore, HAADF-STEM imaging showed degradation of the L-AgNW morphology, including hollowing out of the wires and the presence of several irregular particles surrounding them (Figure 4a, b). Similar to S-AgNWs, elemental analysis of L-AgNWs internalized in HMMs (Figure 4e, f) by STEM-EDX showed that the Ag core of L-AgNWs (red) was surrounded by a sulfur-rich shell (green).

Cellular uptake of L-AgNWs by confocal microscopy

Since 3D HAADF-STEM tomography had revealed that even the longer nanowires (L-AgNWs) could be completely internalized by HMMs, we used confocal laser microscopy to provide further insights into their uptake and processing. The uptake of 25 μg/mL of L-AgNWs by confocal laser microscopy was carried out in conjunction with a fixable lysotracker dye, to perform a lysosomal co-localization study. AgNMs have the capacity to reflect light, therefore their uptake by cells can be monitored by confocal microscopy directly, *i.e.* without the use of

fluorescent labelling of the AgNMs. After 2 h of incubation, most HMMs contained several L-AgNWs within the cytoplasm as well as surface-bound or partially ingested L-AgNWs (Figure 5a; overlay of maximum intensity projection; a z-stack movie of Figure 5a is provided in the Supplementary Information). In some cases L-AgNWs were observed in close proximity to the nucleus (Figure 5b, frame overlay taken at the height of the nucleus). AgNWs did not enter the nucleus as close inspection of the individual frames acquired at the height of the nucleus show that AgNWs overlay the nucleus in the cytoplasmic layer, but do not go through it. Most L-AgNWs were surrounded by a multitude of lysosomes. Figure 5b shows a long AgNW inside the cell (arrow), very close to a large lysosome (arrowhead); actual co-localization, however, was not observed. This lack of co-localization detection of L-AgNWs with lysosomes could be due to a slow delivery of large L-AgNWs to the lysosomes due to their size. Co-localization detection may also have been hindered by fast intracellular degradation of AgNWs (< 2 h, as demonstrated by HAADF-STEM, Figure 3a-b), which could alter the reflectance properties of the particles.

Discussion

The aim of the present study was to examine whether the toxicity of intracellular AgNWs can be correlated to the amount of bioavailable/intracellular Ag^+ ions, as well as to establish whether and how AgNWs degrade inside primary human macrophages, using 1.5 and 10.5 μm-long AgNWs. There has been much discussion in the literature on AgNM toxicity to cells and as to whether this reactivity arises due to ionic or particulate effects, or both.[26] In the case of high-aspect ratio AgNWs, previous studies have pointed towards frustrated phagocytosis of AgNWs by alveolar macrophages as an important factor contributing to the onset of inflammatory

potential.[5, 8] However, the mechanisms by which fully ingested AgNWs transform within primary macrophage cells have not been sufficiently investigated.

In the present study, the cell viability of HMMs varied with the size of the different AgNMs tested, with LC_{50} values ranging from about 0.1 to 60 μg/mL. Similar to our study, a dependence of cell viability on particle size has been demonstrated for mouse macrophages exposed to AgNPs, with IC_{50} values in the range of around 5-20 μg/ml.[27] However, studies on the toxicity of AgNMs to different types of macrophage cells have come to varied conclusions. This variability has been assumed to be caused by different rates of intracellular dissolution of metallic Ag(0) to soluble ionic Ag-species,[14] among AgNMs of different sizes. For smaller particle sizes, AgNP toxicity has been suggested to be mediated by the fast intracellular release of ionic Ag^+, whereas for larger particles, dominated by interaction with the metallic nano-Ag due to slower Ag^+ release.[27, 28]

Nonetheless, what many studies in the literature examining AgNM toxicity may not be taking into account is the total amount of AgNM actually ingested by the cells, which in our view is extremely important when comparing the cytotoxicity of different compounds or different cell types. The amount of AgNMs taken up by cells would be determined by the cellular uptake mechanism, which has a complex interplay with several physical properties of the NM, such as particle size, shape or surface charge.[29] *In vivo*, following AgNW inhalation and alveolar deposition, the amount of AgNMs taken up by cells may also be modulated by the pulmonary surfactant (PS), which is a complex mixture of lipids (mainly phospholipids) and surfactant specific proteins (SP-A, B, C and D) covering the alveolar surface. For instance, phospholipid coatings on single walled carbon nanotubes facilitated their recognition and internalization by *murine* macrophages.[30] In contrast, in our own work, human alveolar type II cell secretions

reduced AgNW bioreactivity with human alveolar type-I like (TT1) cells by reducing their uptake, possibly involving specific binding of SP-A/D to the AgNWs,[31] which we have found induces AgNW agglomeration.[16] The applicability of these findings on HMMs remain to be established, but they stress out the importance of quantifying the active uptake of AgNMs within cells for accurate comparisons of cytotoxicity.

In our present experiment in HMMs, a strong linear correlation between the cellular Ag-content after active uptake and the measured LC_{50}-values was found, for all types of Ag materials tested. This correlation implies that, intracellularly, Ag^+ must be released at a similar rate by all Ag materials tested. The notion that free Ag^+ ions - rather than metallic Ag - are the toxic species for mammalian cells is widely supported by previous studies. In A549 cells, the cytotoxic effect of AgNPs was partly reversed by incubation of cells with the general metal chelator BAL (Dimercaprol),[32] while Ag nanoclusters with a high Ag^+ release rate were more cytotoxic to human fibroblasts than Ag nanoclusters with low Ag^+-release rate.[33] Exactly how the released Ag^+ exerts its cytotoxicity is an area of active study, extensively discussed in the literature,[34] but intracellular dissolution is thought to occur due to the lower pH in the acidic environment of the lysosomes.[35] Accordingly, treatment of the cells with ammonium chloride (NH_4Cl), which brings lysosomal pH to neutral levels, prevented Ag-induced intracellular ROS production and restored cell viability.[36] In another work, introduction of Au-, Ag- and Fe_3O_4-metal NPs directly into the cytosol of cells using a pneumatic gun – and thereby avoiding lysosomal acidic pH and dissolution - produced much less cytotoxicity compared to uptake via the endosomal-lysosomal route, which indicates that acid-facilitated release of reactive metal ions in the lysosomes following uptake may be a general mechanism for metal NP cytotoxicity.[37]

Our co-localization confocal study using the lysotracker dye provided no evidence of actual co-localization of L-AgNW with lysosomes, but numerous lysosomal vesicles were always observed in close vicinity to the nanowires. Many previous studies found spherical AgNPs located in lysosomes.[14, 28, 32, 36] The lack of co-localization detection in our work was probably due to the larger size of L-AgNWs, which are more likely to be internalized by phagocytosis or macropinocytosis, a specialized form of the endocytic pathway particularly active in macrophages and dendritic cells.[38] Ultimately, phagosomes and macropinosomes are thought to fuse with lysosomes in most cell types,[38] explaining the frequent appearance of lysosomes in the vicinity of AgNWs. In addition, as delivery of the AgNWs to the lysosomes would quickly lead to degradation of AgNWs in the acidic environment and alter their reflectance properties, the time window to observe actual co-localization would be brief.

In an attempt to model free ionic Ag^+ and compare its effects to metallic Ag, we exposed HMMs to $AgNO_3$. However, we found that, upon addition to the tissue culture medium, free Ag^+ was almost entirely sequestered by chloride and sulfide components of the media formulation, to form a mixture of AgCl and Ag_2S nanoparticles. On the one hand, this finding highlights the importance of thorough characterization of the materials tested, in order to accurately understand which particulate species actually interact with the cells. On the other hand, we found that this AgCl/Ag_2S precipitate was highly toxic to the cells, in spite of the low dissolution rates measured in the abiotic dissolution assay using perchlorate buffers. This suggests that intracellular dissolution of these particles in HMMs may occur. In the case of Ag_2S, its ultralow solubility product constant ($K_{sp} = 5.92\times10^{-51}$), indicates that a minimal amount of Ag^+ is expected to be released, leading to very low toxicity. Indeed, Ag_2S quantum dots had negligible effects in altering cell proliferation, triggering apoptosis and necrosis, generating reactive oxygen

species, or causing DNA damage in mouse fibroblast L929 cells.[39] AgCl however, although very insoluble in water ($K_{sp} = 1.77\times10^{-10}$), can dissolve in solutions containing specific ligands, including chloride (Cl^-), the most abundant anion in living organisms. Depending on the levels of Cl^-, bioavailable anionic Ag complexes such as $AgCl_2^-$, $AgCl_3^{2-}$, or $AgCl_4^{3-}$ may be formed, possibly increasing toxicity.[17] In one study, for example, the inhibition of nitrifying bacterial growth by AgCl colloids was as significant as Ag^+ ion inhibition.[40]

Our 3D HAADF-STEM tomography and confocal data showed that even the longest AgNWs used in this study could be completely ingested by the HMMs. However, we observed structural changes in internalized AgNWs, compared to the as-synthesized AgNWs, with precipitation of AgCl and Ag_2S compounds. Together with our confocal study, this indicates that AgNWs likely degrade in the acidic pH of the lysosomal and/or phagolysosomal/macropinocytic compartment of HMMs. This intracellular dissolution and reprecipitation could result in a disintegration of their original structure and their fragmentation into shorter parts, similar to what we have previously measured *in vivo* in alveolar epithelial Type II (ATII) cells.[9] Furthermore, this process must involve at least transient release of highly reactive free Ag^+ ions, a portion of which could be a possible source of toxicity towards HMMs. In contrast to our previous work, where internalization of AgNWs in human alveolar epithelial type-I like (TT1) cells only resulted in precipitation of Ag_2S,[13] AgCl precipitation was also observed in HMMs. This could be due to the fact that macrophages are phagocytic cells, programmed to engulf and digest foreign substances, which includes the phagosomal production of highly reactive hypochlorous acid (HOCl) and N-chloramines (RNCl).[41] Consequently, rapid formation of AgCl precipitates in HMMs was observed at the earliest time point of ingestion, but after 24 h and 7 days, AgCl gradually became non-detectable. These findings may indicate that intracellular dissolution of AgCl, as

hypothesized for the $AgNO_3$/medium precipitate, could be another likely mechanism of toxicity for AgNWs in HMMs.

Sulfidation of AgNWs is a complex process which may occur *via* two chemical pathways, depending on the sulfide concentration in the cellular microenvironment. For low sulfide concentrations (< 0.025 μg/mL), sulfidation is dominated by an indirect reaction, *i.e.* oxidative dissolution of silver followed by sulfide precipitation.[42] In this case, an asymmetric behavior as was observed in our experiments may be expected, with faster sulfidation at the ends of AgNWs, which have higher surface energy and density of surface defects. At higher sulfide concentrations, the mechanism switches to a direct oxysulfidation reaction, where the reaction rate increases with increasing sulfide concentration. Dynamic protein adsorption on the surface of AgNPs, may also be an important modulator in their sulfidation process, with strongly attached protein corona acting as a site for sulfidation.[43] The dissolution of AgNWs in the presence of chloride is currently not well-understood. For AgNPs, dissolution was inversely proportional to the Ag/Cl ratio, with decreasing Ag/Cl increasing dissolution.[44] Consequently, the dissolution process of AgNWs in aerobic systems and in the presence of Cl^- would also be difficult to predict, because the precipitation of AgCl, or dissolution and formation of $AgCl_x^{(x-1)-}$, makes dissolution rate a complicated function of Cl^- concentration. These complex intracellular dissolution processes suggest that simple abiotic dissolution assays, like the one used in this work, may be poor predictors of the potential cytotoxicity of AgNMs.

In summary, our study suggests that the toxicity of AgNMs to HMMs is governed by their degree of active cell uptake and subsequent intracellular dissolution and transformation. This held true for AgNM compounds as diverse as $AgNO_3$/medium precipitates, spherical $AgNP_{50}$ and short and long AgNWs. Using a combination of analytical TEM and optical

microscopy techniques, we demonstrated that even extremely long AgNWs could be taken up by HMMs completely, and are degraded intracellularly following uptake, leading to the precipitation of AgCl as well as Ag_2S. These transformation processes likely take place because AgNWs are unstable in the acidic pH of lysosomes, leading to the release of reactive Ag^+ ions that rapidly react with Cl- and SH- groups of the cell microenvironment. A fraction of the free ionic Ag^+ released during this transformation process, as well as subsequent intracellular dissolution of the AgCl formed, may be possible sources of AgNW cytotoxicity to HMMs.

Table 1: Summary of the physicochemical characteristics of silver nanowires ("short": S-AgNWs and "long": L-AgNWs) and 50 nm silver nanoparticles ($AgNP_{50}$), in de-ionized (DI) water and serum-free RPMI tissue culture medium.

	S-AgNWs	**L-AgNWs**	**$AgNP_{50}$**
Size (TEM)	Diameter 79 nm (36-108 nm); Length 1.5 μm (0.1-3.1 μm)	Diameter 73 nm (42-128 nm) Length 10.5 μm (0.2-35μm)	Diameter 54 ± 20 nm
Capping Agent	PVP (poly(vinyl pyrrolidone); $M_w \approx 360k$)	PVP (poly(vinyl pyrrolidone); $M_w \approx 360k$)	Citrate (sodium citrate)
ζ-potential (DI water)	- 14.8 ± 0.1 mV	-15.2 ± 0.2 mV	- 27.8 ± 0.1 mV
ζ-potential (RPMI, pH7.2)	-8.4 ± 0.6 mV	-8.7 ± 0.5 mV	-23.0 ± 0.8

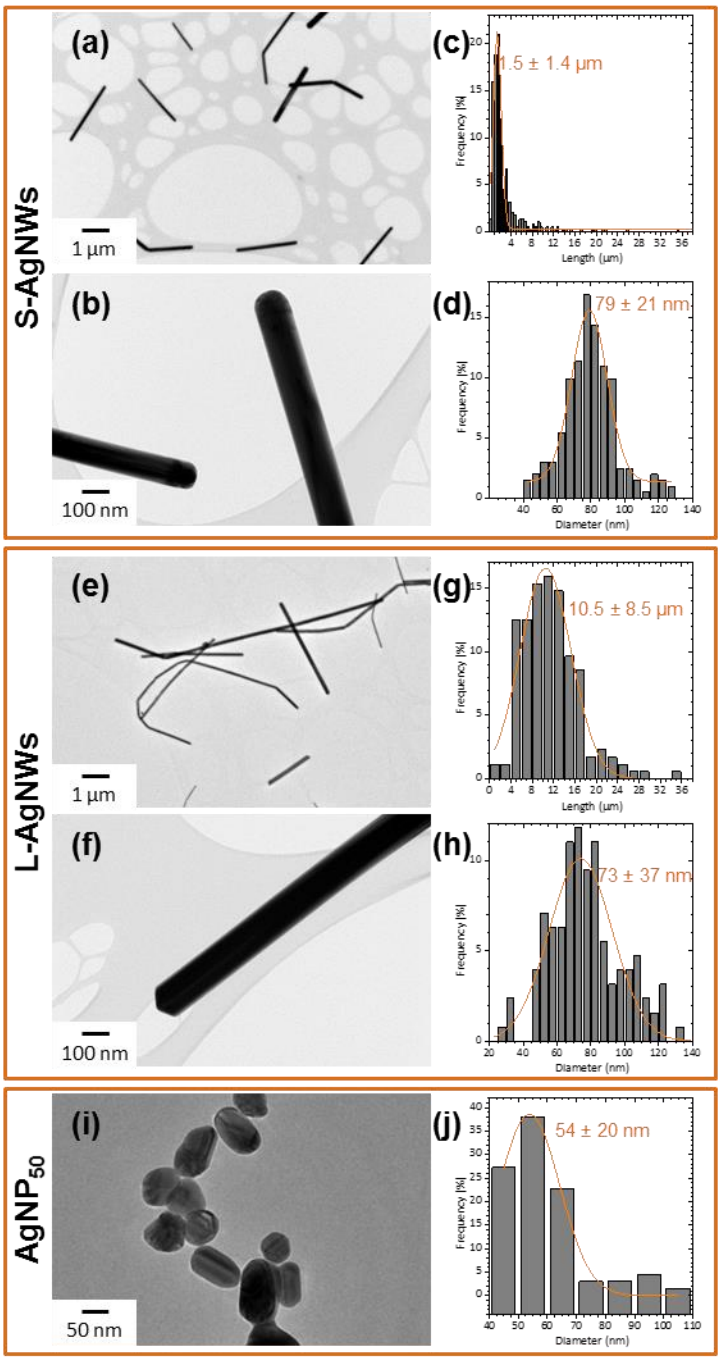

Figure 1. Characterization of as-synthesized AgNMs. Bright field transmission electron microscopy (BF-TEM) images of S-AgNWs (a, b) and L-AgNWs (e, f) and their length (c, g) and diameter (d, h) distributions. (i) BF-TEM image of $AgNP_{50}$ and their diameter (j) distribution. The curves in (c, d, g, h, j) represent the Gaussian fit to the data.

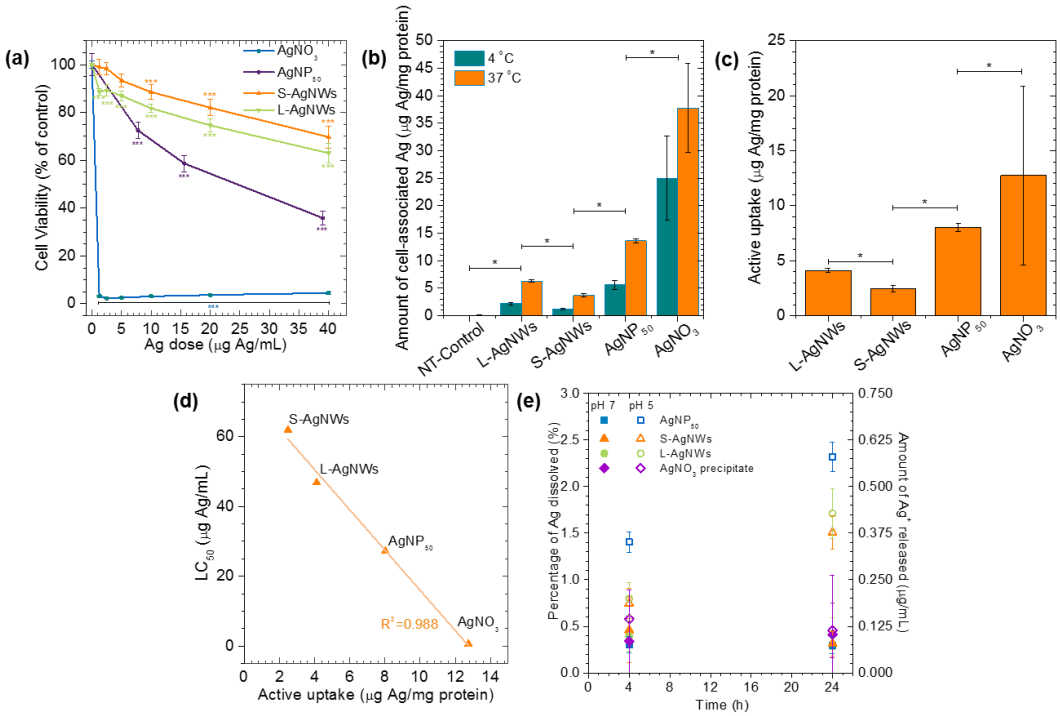

Figure 2. (a) Cell viability of human monocyte-derived macrophages (HMMs) following a 24 h treatment with 0 to 40 μg/mL of $AgNO_3$, $AgNP_{50}$, S-AgNWs and L-AgNWs. Cell viability was measured by the MTT assay and data is presented as a ratio (%) compared to the non-treated (NT) control ± standard error (SE) (n=3). (b) Inductively coupled plasma optical emission spectroscopy (ICP-OES) quantification of Ag amounts associated with HMMs, treated for 4 h with 10 μg/mL of $AgNO_3$, $AgNP_{50}$, S-AgNWs or L-AgNWs, at 4 ºC or 37 ºC. The data was normalized to cellular protein content and is presented as mean ± SE (n=5). (c) Active uptake of Ag compounds by HMMs, calculated by the difference in Ag amounts associated with cells at 37 ºC and 4 ºC. (d) Correlation of the active uptake with cell cytotoxicity (LC_{50} values estimated from the MTT assay). The solid line represents a linear correlation to the data. (e) ICP-OES analysis of the percentage and amount of free Ag^+ ions released from $AgNP_{50}$, S-AgNWs, L-AgNWs and the $AgNO_3$ precipitate (obtained by the addition of $AgNO_3$ in MΦ-SFM cell culture medium), incubated in perchlorate buffer solutions with pH 7 (solid symbols) and pH 5 (hollow symbols), for 4 and 24 h.

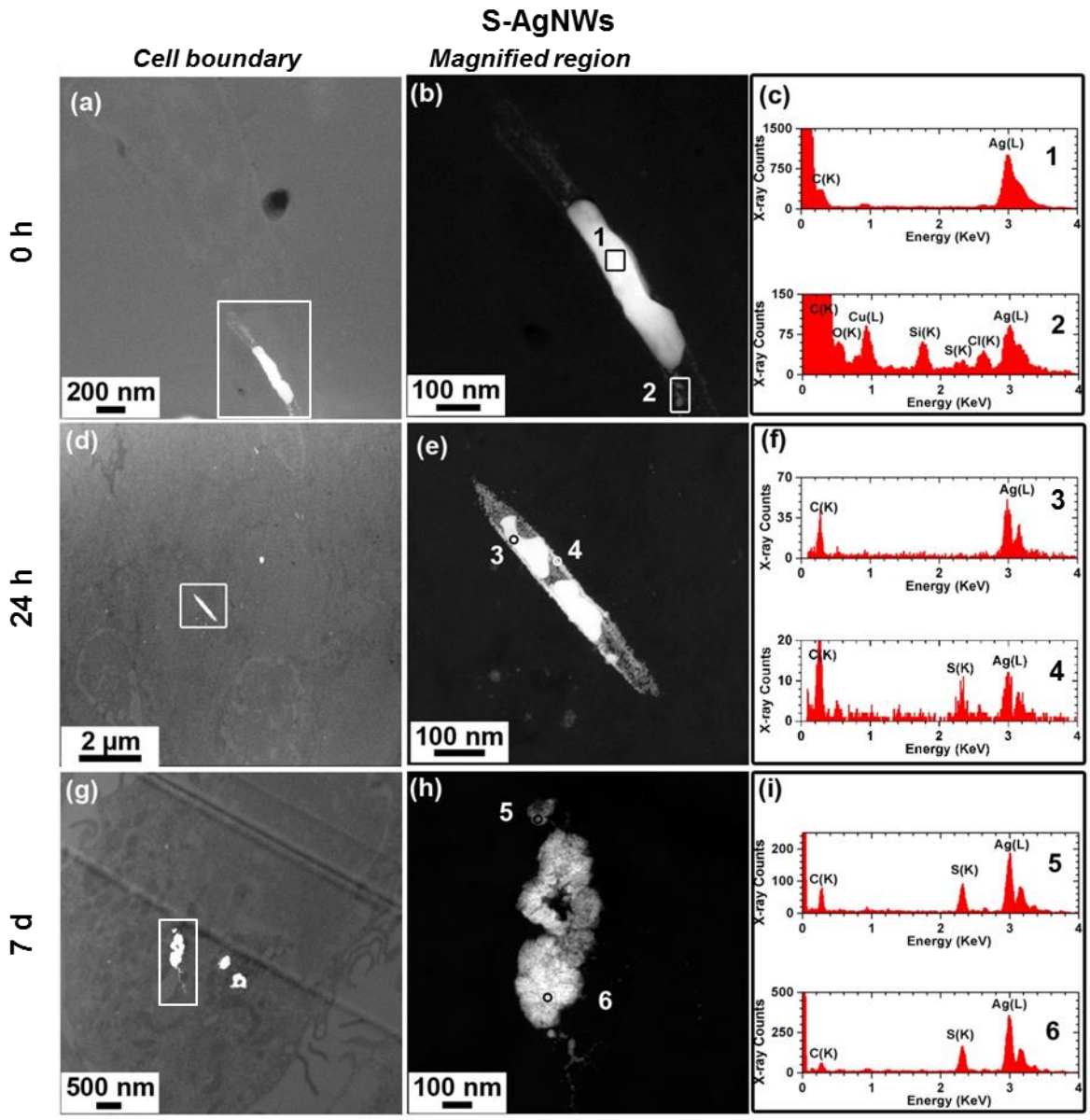

Figure 3. Changes in the morphology and composition of S-AgNWs in HMMs as a function of time: at the 0-h time point (immediately after the 2 h pulse period; a–c), and after chase periods of 24 h (d–f) or 7 d (g–i). (a, d, g) High angle annular dark field scanning transmission electron microscopy (HAADF-STEM) images of S-AgNWs inside HMMs in unstained ultrathin sections; (b, e, h) are magnifications of the areas boxed in (a, d, g). (c, f, i) STEM energy dispersive X-ray (STEM-EDX) spectra collected from the corresponding areas marked in (b, e, h).

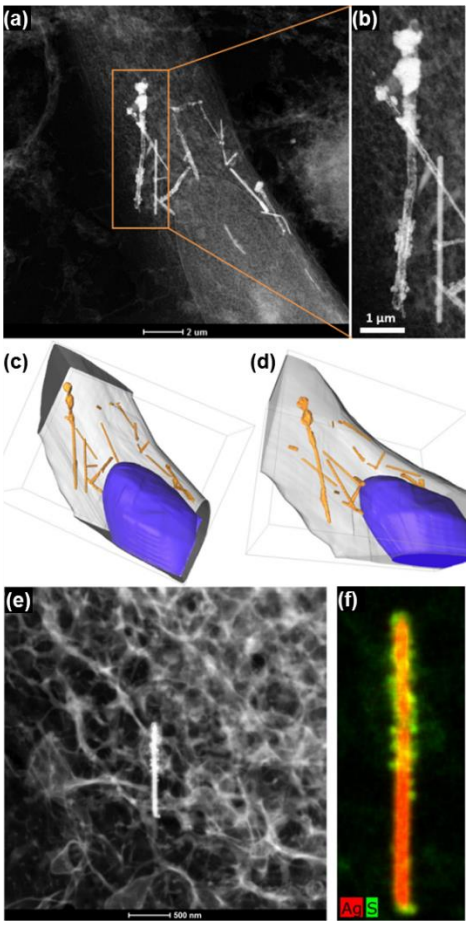

Figure 4. (a) HAADF-STEM imaging of L-AgNWs in a freeze-dried HMM cell, showing internalization of L-AgNWs and degradation of their morphologies, including hollowing of the nanowires and presence of a rough granular shell surrounding the nanowires. (b) Magnification of the area boxed in (a). (c, d) Visualizations from two angles of a tomographic reconstruction of the cell imaged in (a), showing the 3D distribution of L-AgNWs (orange) with respect to the plasma membrane (grey) and the cell nucleus (blue). (e) HAADF-STEM image of L-AgNWs associated with a HMM cell and (b) elemental maps generated from STEM-EDX analysis of the same nanowire, showing a Ag-rich nanowire core (red) surrounded in parts by a granular sulfur-rich shell (green).

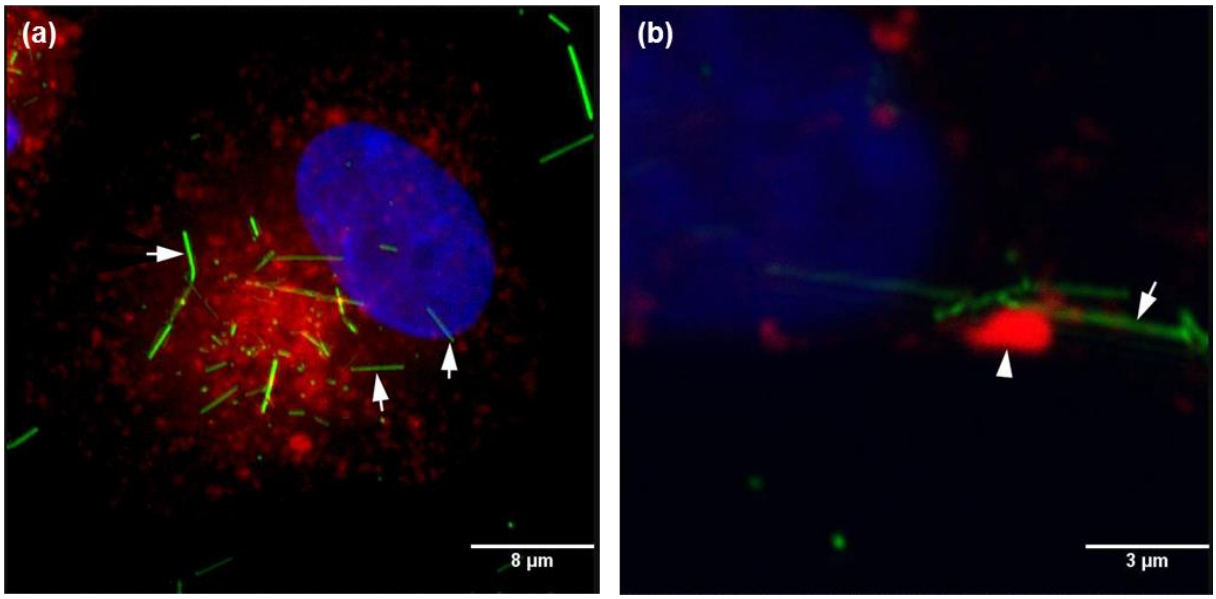

Figure 5. Confocal imaging of L-AgNW uptake by HMMs and co-localization with lysosomes. Cells were incubated with 25 µg/mL of L-AgNWs for 2 h at 37 ºC in the presence of 10 k-dextran-TexasRed (a lysosomal tracker; red). L-AgNWs were imaged in reflectance mode (green), while cell nuclei were counterstained with Hoechst (blue). Images show overlays of single frames acquired at the height of the nucleus.

ASSOCIATED CONTENT

Supporting Information. Supplementary figures. The following files are available free of charge. Supporting Information (PDF)

AUTHOR INFORMATION

Corresponding Authors

*M.P.R: Phone: (+44)2075946755; fax: (+44)2075945017; e-mail: m.p.ryan@imperial.ac.uk.

*A.E.P. Phone: (+44)2075949691; fax: (+44)2075945017; e-mail: a.e.porter@imperial.ac.uk

Author Contributions

The manuscript was written through contributions of all authors. All authors have given approval to the final version of the manuscript. ‡These authors contributed equally.

REFERENCES

1. Melosh, N. A.; Boukai, A.; Diana, F.; Gerardot, B.; Badolato, A.; Petroff, P. M.; Heath, J. R. Ultrahigh-density nanowire lattices and circuits. *Science* **2003**, 300, 112-5.

2. Park, J.; Kwak, B. K.; Bae, E.; Lee, J.; Kim, Y.; Choi, K.; Yi, J. Characterization of exposure to silver nanoparticles in a manufacturing facility. *Journal of Nanoparticle Research* **2009**, 11, 1705-1712.

3. George, S.; Lin, S. J.; Jo, Z. X.; Thomas, C. R.; Li, L. J.; Mecklenburg, M.; Meng, H.; Wang, X.; Zhang, H. Y.; Xia, T.; Hohman, J. N.; Lin, S.; Zink, J. I.; Weiss, P. S.; Nel, A. E. Surface Defects on Plate-Shaped Silver Nanoparticles Contribute to Its Hazard Potential in a Fish Gill Cell Line and Zebrafish Embryos. *ACS Nano* **2012**, 6, 3745-3759.

4. Scanlan, L. D.; Reed, R. B.; Loguinov, A. V.; Antczak, P.; Tagmount, A.; Aloni, S.; Nowinski, D. T.; Luong, P.; Tran, C.; Karunaratne, N.; Pham, D.; Lin, X. X.; Falciani, F.; Higgins, C. P.; Ranville, J. F.; Vulpe, C. D.; Gilbert, B. Silver Nanowire Exposure Results in Internalization and Toxicity to Daphnia magna. *ACS Nano* **2013**, 7, 10681-10694.

5. Schinwald, A.; Donaldson, K. Use of back-scatter electron signals to visualise cell/nanowires interactions in vitro and in vivo; frustrated phagocytosis of long fibres in macrophages and compartmentalisation in mesothelial cells in vivo. *Particle and Fibre Toxicology* **2012**, 9, 34.

6. Stoehr, L. C.; Gonzalez, E.; Stampfl, A.; Casals, E.; Duschl, A.; Puntes, V.; Oostingh, G. J. Shape matters: effects of silver nanospheres and wires on human alveolar epithelial cells. *Particle and Fibre Toxicology* **2011**, 8, 36.

7. Sturm, R.; Hofmann, W. A theoretical approach to the deposition and clearance of fibers with variable size in the human respiratory tract. *Journal of Hazardous Materials* **2009**, 170, 210-218.

8. Silva, R. M.; Xu, J.; Saiki, C.; Anderson, D. S.; Franzi, L. M.; Vulpe, C. D.; Gilbert, B.; Van Winkle, L. S.; Pinkerton, K. E. Short versus long silver nanowires: a comparison of in vivo pulmonary effects post instillation. *Particle and Fibre Toxicology* **2014**, 11, 52.

9. Chung, K. F.; Seiffert, J.; Chen, S.; Theodorou, I. G.; Goode, A. E.; Leo, B. F.; McGilvery, C. M.; Hussain, F.; Wiegman, C.; Rossios, C.; Zhu, J.; Gong, J.; Tariq, F.; Yufit, V.; Monteith, A. J.; Hashimoto, T.; Skepper, J. N.; Ryan, M. P.; Zhang, J.; Tetley, T. D.; Porter, A. E. Inactivation, Clearance, and Functional Effects of Lung-Instilled Short and Long Silver Nanowires in Rats. *ACS Nano* **2017**.

10. Donaldson, K.; Murphy, F.; Schinwald, A.; Duffin, R.; Poland, C. A. Identifying the pulmonary hazard of high aspect ratio nanoparticles to enable their safety-by-design. *Nanomedicine* **2011**, 6, 143-56.

11. Donaldson, K.; Murphy, F.; Duffin, R.; Poland, C. Asbestos, carbon nanotubes and the pleural mesothelium: a review of the hypothesis regarding the role of long fibre retention in the parietal pleura, inflammation and mesothelioma. *Particle and Fibre Toxicology* **2010**, 7, 5.

12. Schinwald, A.; Chernova, T.; Donaldson, K. Use of silver nanowires to determine thresholds for fibre length-dependent pulmonary inflammation and inhibition of macrophage migration in vitro. *Particle and Fibre Toxicology* **2012**, 9, 47.

13. Chen, S.; Goode, A. E.; Sweeney, S.; Theodorou, I. G.; Thorley, A. J.; Ruenraroengsak, P.; Chang, Y.; Gow, A.; Schwander, S.; Skepper, J.; Zhang, J. J.; Shaffer, M. S.; Chung, K. F.; Tetley, T. D.; Ryan, M. P.; Porter, A. E. Sulfidation of silver nanowires inside human alveolar epithelial cells: a potential detoxification mechanism. *Nanoscale* **2013**, 5, 9839-47.

14. Wang, L.; Zhang, T.; Li, P.; Huang, W.; Tang, J.; Wang, P.; Liu, J.; Yuan, Q.; Bai, R.; Li, B.; Zhang, K.; Zhao, Y.; Chen, C. Use of Synchrotron Radiation-Analytical Techniques To Reveal Chemical Origin of Silver-Nanoparticle Cytotoxicity. *ACS Nano* **2015**, 9, 6532-47.

15. Veronesi, G.; Aude-Garcia, C.; Kieffer, I.; Gallon, T.; Delangle, P.; Herlin-Boime, N.; Rabilloud, T.; Carriere, M. Exposure-dependent Ag+ release from silver nanoparticles and its complexation in AgS2 sites in primary murine macrophages. *Nanoscale* **2015**, 7, 7323-7330.

16. Theodorou, I. G.; Botelho, D.; Schwander, S.; Zhang, J.; Chung, K. F.; Tetley, T. D.; Shaffer, M. S.; Gow, A.; Ryan, M. P.; Porter, A. E. Static and Dynamic Microscopy of the

Chemical Stability and Aggregation State of Silver Nanowires in Components of Murine Pulmonary Surfactant. *Environmental Science & Technology* **2015**, 49, 8048-56.

17. Levard, C.; Hotze, E. M.; Lowry, G. V.; Brown, G. E., Jr. Environmental Transformations of Silver Nanoparticles: Impact on Stability and Toxicity. *Environmental Science & Technology* **2012**, 46, 6900-6914.

18. Muller, K.; Skepper, J. N.; Tang, T. Y.; Graves, M. J.; Patterson, A. J.; Corot, C.; Lancelot, E.; Thompson, P. W.; Brown, A. P.; Gillard, J. H. Atorvastatin and uptake of ultrasmall superparamagnetic iron oxide nanoparticles (Ferumoxtran-10) in human monocyte-macrophages: implications for magnetic resonance imaging. *Biomaterials* **2008**, 29, 2656-62.

19. Chen, S.; Theodorou, I. G.; Goode, A. E.; Gow, A.; Schwander, S.; Zhang, J.; Chung, K. F.; Tetley, T. D.; Shaffer, M. S.; Ryan, M. P.; Porter, A. E. High-Resolution Analytical Electron Microscopy Reveals Cell Culture Media-Induced Changes to the Chemistry of Silver Nanowires. *Environmental Science & Technology* **2013**, 47, 13813-13821.

20. Fatisson, J.; Quevedo, I. R.; Wilkinson, K. J.; Tufenkji, N. Physicochemical characterization of engineered nanoparticles under physiological conditions: Effect of culture media components and particle surface coating. *Colloids and Surfaces B: Biointerfaces* **2012**, 91, 198-204.

21. Eckhardt, S.; Brunetto, P. S.; Gagnon, J.; Priebe, M.; Giese, B.; Fromm, K. M. Nanobio Silver: Its Interactions with Peptides and Bacteria, and Its Uses in Medicine. *Chemical Reviews* **2013**, 113, 4708-4754.

22. Wittmaack, K. Excessive delivery of nanostructured matter to submersed cells caused by rapid gravitational settling. *ACS Nano* **2011**, 5, 3766-78.

23. Creuwels, L. A.; van Golde, L. M.; Haagsman, H. P. The pulmonary surfactant system: biochemical and clinical aspects. *Lung* **1997**, 175, 1-39.

24. Parra, E.; Pérez-Gil, J. Composition, structure and mechanical properties define performance of pulmonary surfactant membranes and films. *Chemistry and Physics of Lipids* **2015**, 185, 153-175.

25. Ivask, A.; ElBadawy, A.; Kaweeteerawat, C.; Boren, D.; Fischer, H.; Ji, Z.; Chang, C. H.; Liu, R.; Tolaymat, T.; Telesca, D.; Zink, J. I.; Cohen, Y.; Holden, P. A.; Godwin, H. A. Toxicity Mechanisms in Escherichia coli Vary for Silver Nanoparticles and Differ from Ionic Silver. *ACS Nano* **2013**, 8, 374-386.

26. Theodorou, I.; Ryan, M.; Tetley, T.; Porter, A. Inhalation of Silver Nanomaterials—Seeing the Risks. *International Journal of Molecular Sciences* **2014**, 15, 23936-23974.

27. Pratsinis, A.; Hervella, P.; Leroux, J.-C.; Pratsinis, S. E.; Sotiriou, G. A. Toxicity of Silver Nanoparticles in Macrophages. *Small* **2013**, 9, 2576-2584.

28. Arai, Y.; Miyayama, T.; Hirano, S. Difference in the toxicity mechanism between ion and nanoparticle forms of silver in the mouse lung and in macrophages. *Toxicology* **2015**, 328, 84-92.

29. Tay, C. Y.; Setyawati, M. I.; Xie, J.; Parak, W. J.; Leong, D. T. Back to Basics: Exploiting the Innate Physico-chemical Characteristics of Nanomaterials for Biomedical Applications. *Advanced Functional Materials* **2014**, 24, 5936-5955.

30. Konduru, N. V.; Tyurina, Y. Y.; Feng, W.; Basova, L. V.; Belikova, N. A.; Bayir, H.; Clark, K.; Rubin, M.; Stolz, D.; Vallhov, H.; Scheynius, A.; Witasp, E.; Fadeel, B.; Kichambare, P. D.; Star, A.; Kisin, E. R.; Murray, A. R.; Shvedova, A. A.; Kagan, V. E. Phosphatidylserine Targets Single-Walled Carbon Nanotubes to Professional Phagocytes In Vitro and In Vivo. *PLoS ONE* **2009**, 4, e4398.

31. Sweeney, S.; Theodorou, I. G.; Zambianchi, M.; Chen, S.; Gow, A.; Schwander, S.; Zhang, J. J.; Chung, K. F.; Shaffer, M. S.; Ryan, M. P.; Porter, A. E.; Tetley, T. D. Silver nanowire interactions with primary human alveolar type-II epithelial cell secretions: contrasting bioreactivity with human alveolar type-I and type-II epithelial cells. *Nanoscale* **2015**.

32. De Matteis, V.; Malvindi, M. A.; Galeone, A.; Brunetti, V.; De Luca, E.; Kote, S.; Kshirsagar, P.; Sabella, S.; Bardi, G.; Pompa, P. P. Negligible particle-specific toxicity mechanism of silver nanoparticles: the role of Ag+ ion release in the cytosol. *Nanomedicine* **2015**, 11, 731-9.

33. Hamilton, R. F., Jr.; Buckingham, S.; Holian, A. The Effect of Size on Ag Nanosphere Toxicity in Macrophage Cell Models and Lung Epithelial Cell Lines Is Dependent on Particle Dissolution. *International Journal of Molecular Sciences* **2014**, 15, 6815-6830.

34. Dubey, P.; Matai, I.; Kumar, S. U.; Sachdev, A.; Bhushan, B.; Gopinath, P. Perturbation of cellular mechanistic system by silver nanoparticle toxicity: Cytotoxic, genotoxic and epigenetic potentials. *Advances in Colloid and Interface Science* **2015**, 221, 4-21.

35. Wang, X.; Ji, Z.; Chang, C. H.; Zhang, H.; Wang, M.; Liao, Y.-P.; Lin, S.; Meng, H.; Li, R.; Sun, B.; Winkle, L. V.; Pinkerton, K. E.; Zink, J. I.; Xia, T.; Nel, A. E. Use of Coated Silver Nanoparticles to Understand the Relationship of Particle Dissolution and Bioavailability to Cell and Lung Toxicological Potential. *Small* **2014**, 10, 385-398.

36. Setyawati, M. I.; Yuan, X.; Xie, J.; Leong, D. T. The influence of lysosomal stability of silver nanomaterials on their toxicity to human cells. *Biomaterials* **2014**, 35, 6707-15.

37. Guarnieri, D.; Sabella, S.; Muscetti, O.; Belli, V.; Malvindi, M. A.; Fusco, S.; De Luca, E.; Pompa, P. P.; Netti, P. A. Transport across the cell-membrane dictates nanoparticle fate and toxicity: a new paradigm in nanotoxicology. *Nanoscale* **2014**, 6, 10264-73.

38. Lim, J. P.; Gleeson, P. A. Macropinocytosis: an endocytic pathway for internalising large gulps. *Immunology and Cell Biology* **2011**, 89, 836-43.

39. Zhang, Y.; Hong, G.; Zhang, Y.; Chen, G.; Li, F.; Dai, H.; Wang, Q. Ag2S Quantum Dot: A Bright and Biocompatible Fluorescent Nanoprobe in the Second Near-Infrared Window. *ACS Nano* **2012**, 6, 3695-3702.

40. Choi, O.; Deng, K. K.; Kim, N.-J.; Ross Jr, L.; Surampalli, R. Y.; Hu, Z. The inhibitory effects of silver nanoparticles, silver ions, and silver chloride colloids on microbial growth. *Water Research* **2008**, 42, 3066-3074.

41. Roos, D. The involvement of oxygen radicals in microbicidal mechanisms of leukocytes and macrophages. *Klinische Wochenschrift* **1991**, 69, 975-80.

42. Liu, J.; Pennell, K. G.; Hurt, R. H. Kinetics and mechanisms of nanosilver oxysulfidation. *Environmental Science & Technology* **2011**, 45, 7345-53.

43. Miclaus, T.; Beer, C.; Chevallier, J.; Scavenius, C.; Bochenkov, V. E.; Enghild, J. J.; Sutherland, D. S. Dynamic protein coronas revealed as a modulator of silver nanoparticle sulphidation in vitro. *Nature Communications* **2016**, 7, 11770.

44. Li, X. A.; Lenhart, J. J.; Walker, H. W. Dissolution-Accompanied Aggregation Kinetics of Silver Nanoparticles. *Langmuir* **2010**, 26, 16690-16698.

TOC